Journal of the Air & Waste Management Association

Publication details, including instructions for authors and subscription information: http://www.tandfonline.com/loi/uawm20

A Laboratory Study of Sediment and Contaminant Release during Gas Ebullition

Qingzhong Yuan [a] , Kalliat T. Valsaraj [a] , Danny D. Reible [b] & Clinton S. Willson [c]

[a] Gordon A. and Mary Cain Department of Chemical Engineering , Louisiana State University , Baton Rouge , LA , USA

[b] Department of Civil and Environmental Engineering , University of Texas , Austin , TX , USA

[c] Department of Civil and Environmental Engineering , Louisiana State University , Baton Rouge , LA , USA

Published online: 24 Feb 2012.

To cite this article: Qingzhong Yuan , Kalliat T. Valsaraj , Danny D. Reible & Clinton S. Willson (2007) A Laboratory Study of Sediment and Contaminant Release during Gas Ebullition, Journal of the Air & Waste Management Association, 57:9, 1103-1111, DOI: 10.3155/1047-3289.57.9.1103

To link to this article: http://dx.doi.org/10.3155/1047-3289.57.9.1103

TECHNICAL PAPER

ISSN:1047-3289 *J. Air & Waste Manage. Assoc.* **57**:1103–1111
DOI:10.3155/1047-3289.57.9.1103

A Laboratory Study of Sediment and Contaminant Release during Gas Ebullition

Qingzhong Yuan and Kalliat T. Valsaraj
Gordon A. and Mary Cain Department of Chemical Engineering, Louisiana State University, Baton Rouge, LA

Danny D. Reible
Department of Civil and Environmental Engineering, University of Texas, Austin, TX

Clinton S. Willson
Department of Civil and Environmental Engineering, Louisiana State University, Baton Rouge, LA

ABSTRACT

Significant quantities of gas are generated from labile organic matter in contaminated sediments. The implications for the gas generation and subsequent release of contaminants from sediments are unknown but may include enhanced direct transport such as pore water advection and diffusion. The behavior of gas in sediments and the resulting migration of a polyaromatic hydrocarbon, viz phenanthrene, were investigated in an experimental system with methane injection at the base of a sediment column. Hexane above the overlying water layer was used to trap any phenanthrene migrating out of the sediment layer. The rate of suspension of solid particulate matter from the sediment bed into the overlying water layer was also monitored. The experiments indicated that significant amounts of both solid particulate matter and contaminant can be released from a sediment bed by gas movement with the amount of release related to the volume of gas released. The effective mass transfer coefficient of gas bubble-facilitated contaminant release was estimated under field conditions, being around three orders of magnitude smaller than that of bioturbation. A thin sand-capping layer (2 cm) was found to dramatically reduce the amount of contaminant or particles released with the gas because it could prevent or at least reduce sediment suspension. Based on the experimental observations, gas bubble-facilitated contaminant transport pathways for both uncapped and capped systems were proposed. Sediment cores were sliced to obtain phenanthrene concentration. X-ray computed tomography (CT) was used to investigate the void space distribution in the sediment penetrated by gas bubbles. The results showed that gas bubble migration could redistribute the sediment void spaces and may facilitate pore water circulation in the sediment.

IMPLICATIONS

Bubble-facilitated contaminant transport is one of the most important processes in capped sediments. This study shows that partition and sediment suspension are two factors responsible for contaminant transport during bubble ebullition. In field conditions, both gas flux and sediment suspension rates are small, and effective mass transfer coefficients estimated from the experimental data indicate that contaminant release due to gas ebullition is not expected to be significant relative to contaminant release from bioturbation in uncapped sediment. Sand caps are effective in reducing gas bubble-associated contaminant release from sediment. With the help of CT techniques, we observed that bubble movement could redistribute the void spaces and increase pore water circulation in sediment, thus changing the sediment structure and integrity. These results are useful in the cap design.

INTRODUCTION

Contaminated sediments pose a serious challenge in terms of remediation. Although physical removal by dredging is practiced at various locations, this has proven to be less effective than expected or desired, encouraging the development of less-invasive and lower impact in situ approaches. These approaches also present unique challenges because of the variety and complexity of natural processes that occur in situ at the dynamic sediment-water interface. In situ capping is one such method and involves a conceptually simple approach to containment and control of sediment contaminants. However, serious challenges to the application of in situ capping are associated with facilitated transport of contaminants by processes including gas evolution and migration, groundwater seepage, nonaqueous phase liquid (NAPL) presence and movement, and deep dwelling macrofauna that can destabilize the sediment and a cap through bioturbation. Cap placement and subsequent consolidation can destabilize a separate gas or liquid phase previously held by capillary forces. After placement, the development of anaerobic conditions beneath the cap may encourage significant gas generation and mobilization. These gases can migrate out of the sediment into the overlying water and vent to the atmosphere. This facilitated transport is of concern at a number of locations.[1,2] Gas movement has

been demonstrated to be of concern when sediments are contaminated with NAPLs.[3] In this work, we seek to evaluate the potential for contaminant release due to migration in the absence of NAPLs.

Contaminated sediments often contain high organic matter content. Both oxygen profiles and redox potential data show that anaerobic conditions exist in capped sediments.[4] Under anaerobic conditions, organic matter is converted into methane and carbon dioxide by bacterial and microbial activities.[5] Gas bubbles form when the gas reaches saturation in the pore water. Methane gas plumes (so-called gas flares) are found to form on the sea floor.[6] As previously discussed by Martens et al.[7] and Hovland and Judd,[8] the movement of bubbles in sediments may cause a destabilization of the sediment and/or stripping of volatile pollutants out of contaminated sediments and subsequent release into the water column.

Johnson et al.[9] observed that bubbles in sediments are nonspherical and often disk-shaped, with their long axis in a near-vertical orientation. Boudreau et al.[10,11] and Gardiner et al.[12] simulated the process by coupling a reaction-diffusion model to a linear elastic fracture mechanics (LEFM) model. The model results conclude that the bubble growth rate is strongly dependent on bubble aspect ratio and the eccentric bubbles grow two to four times faster than spherical bubbles for an equivalent volume of gas. Furthermore, isolated bubble growth may become arrested so that small bubbles can cease to grow in sediments; isolated bubbles can easily rise in sediments by a buoyancy-driven fracture mechanism. Most recently, they observed that bubbles in sand are essentially spherical away from mud contacts.[13]

A number of papers have been published about gas bubble ebullition rates from wetland sediments, paddy soil, and other sediments.[14–17] The gas fluxes from their observations vary largely from 0.3 to 2640 mL/m^2·day because of the different local conditions. Recently, Himmelheber and Hughes[18] measured the methane generation from Anacostia River sediment in the laboratory and reported that the gas generation rates normalized to sediment-water interfacial area are near 0, 341, and 917 mL/m^2·day at 4, 22 and 35 °C respectively. Fendinger et al.[19] estimated the overall pesticide contaminant fluxes by measuring the gas bubble flux and assuming equilibrium between the gas bubble and water. They noted that because the estimation is only approximate, more research is needed to understand the gas bubble/water partitioning. Huls et al.[2] conducted bench and field studies to investigate the gas generation and the polycyclic aromatic hydrocarbon migration from capped contaminated sediments. They concluded that gas release rates are highly dependent on sediment temperature, and significant insulation will be added to lower sediment temperatures and terminate gas production when a sand cap is placed on the sediment.

As discussed before, nucleation of gas bubbles occurs when gases saturate in the pore water. During their growth, bubbles push aside the surrounding sediment grain matrix. Resulting stresses may initiate cracks around bubbles. If these cracks join, they may form channels stretching to the sediment surface along which gas may escape. Van Kessel et al.[20] reported that accumulation of gas in sludge may continue until a bulk density less than that of water is attained, and only then can gas escape as a result of instabilities in the sediment matrix. The resulting gas movement can influence sediment structure.

X-ray computed tomography (CT) is a nondestructive visualization and characterization technique that creates three-dimensional images that map the variation of X-ray attenuation within objects. The X-ray attenuation is a function of the X-ray energy and the atomic number and density of the material being scanned. Ketcham and Carlson[21] provided an excellent review of the principles of CT and application to geosciences. Because of its nondestructive nature and the large differences in X-ray attenuation between the sediment and the gas bubbles, CT is an excellent tool for investigating the distribution and impact of gas bubbles in sediment systems. Jepsen et al.[22] studied the effects of gas generation on sediment density and erosion. Many others[23,24] have employed CT techniques to investigate the sediment structure nondestructively. The method could capture the influence of gas release on sediment structure.

In this study, a bubble column was used to investigate phenanthrene flux from sediment while injecting methane gas bubbles at the bottom of the column. A hexane layer was placed at the top to collect the material carried by the methane gas bubbles, a process known as solvent sublation.[25,26] Multiple samples from the sediment slurry and hexane were taken during the experimental run. These samples provide contaminant distribution with time in the aqueous phase, hexane, and suspended sediment particles. At the end of the experiment, the sediment in the column was cored. Several of the sediment cores were scanned with CT equipment to determine the void space distribution within the sediment and sand. Finally, all the cores were sliced and analyzed for phenanthrene. Contaminant mass balances were made to assure that the results are reasonable.

MATERIALS AND METHODS

Materials

Phenanthrene of 98% purity as a tracer was purchased from Aldrich Chemicals, Milwaukee, WI.

The sediment used was from the Anacostia River (point 2, Washington, DC) (www.hsrc-ssw.org/anacostia/). The phenanthrene concentration in the original sediment was 0.68 mg/kg (n = 5, SD [standard deviation] = 0.06). The sediment was sieved using a grid with 10 × 10-mm^2 openings. The sieved sediment was inoculated with phenanthrene using a procedure previously described in the literature.[27] The initial phenanthrene concentrations in three samples were 100.1 mg/kg (n = 5, SD = 3), 99.6 mg/kg (n = 5, SD = 0.9) and 102.4 mg/kg (n = 5, SD = 3.3), respectively.

A commercially available sand (QUIKRETE) was employed as the cap in these studies. Before use, it was sieved through two sieves (U.S.A. Standard Testing Sieve Nos. 20 and 70) to remove larger and smaller particles, washed several times with tap water then deionized water, and then dried in the oven at 100 °C.

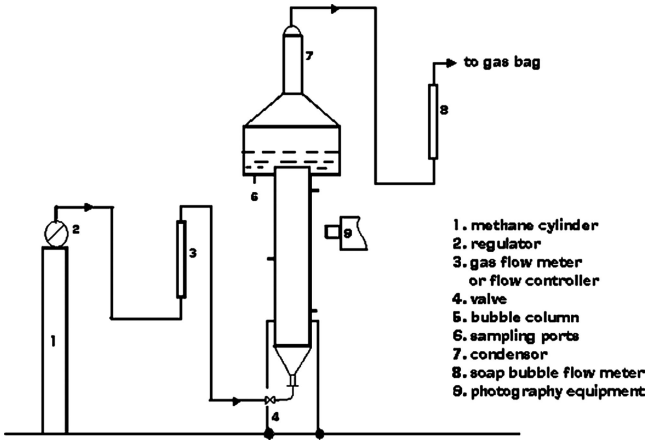

Figure 1. Experimental setup.

Experimental Setup and Operations

Figure 1 is a schematic of the basic experimental setup. The bubble column was a glass column with i.d. of 8 cm and a total height of 74 cm. The gas flow meter (65-mm polytetrafluoroethylene with valve) and volumetric flow controller (0.01–1 mL/min) were purchased from Cole-Parmer.

Contaminated sediment was first added into the bottom of the column. The thickness of the sediment was usually around 20 cm. Then sand (for the capped experiment) and water were slowly and carefully added into the column to minimize mixing and sediment suspension. The height of the water was approximately52 cm. Finally hexane was added on top of the water. The thickness of the hexane layer was 5 cm (~380 g) for flow rates of 0.01 mL/min and capping experiments, and 10 cm (~760 grams) for the other experiments. A cooling condenser was set up and the coolant water pump started to ensure that no hexane evaporative loss occurred. Methane gas from a cylinder was then introduced at the base of the bubble column through a sparger. The gauge pressure of the gas was 100 kPa for all the experiments.

Sample Collection and Measurements

Multiple samples were collected from the water/slurry and hexane layers at several time intervals. The samples from the hexane layer were collected into 2-mL flasks. The hexane was concentrated using a nitrogen blow-down and solvent-exchanged with acetonitrile before high-performance liquid chromatography (HPLC) analysis (U.S. Environmental Protection Agency [EPA] Standard Method 8270).[28] The water samples were collected from sampling ports in the column, placed in 2-mL vials, and directly injected into the HPLC. Slurry samples were collected using a syringe barrel and immediately filtered through a 0.7-μm glass fiber filter (Whatman) to remove the sediment particles. The experimental results showed that phenanthrene sorption to the filter was significant. Extensive tests were conducted to determine the phenanthrene fraction lost at different water-to-dry sediment ratios and phenanthrene aqueous concentrations. Analysis of these tests produced a factor to account for the fraction lost to the filter. The samples from three different heights of the column (bottom, middle, and top) were analyzed at the same time. No significant difference was observed. This suggests that the water/slurry was well mixed by the bubble movement. Total suspended sediment (TSS) was measured by filtration of 4 mL of sediment slurry. The data at several time intervals gave the variation of TSS with time.

After the experiment reached a steady state, the hexane and the slurry layers were drained from the column, and sediment was cored with a transparent plastic tube (diameter = 30 mm). One end of the plastic tube was machined to a thin edge; it was pushed through the sediment until it reaching the sparger at the bottom. A soft tube was utilized to connect the top end of the tube with a self-made piston-cylinder vacuum system. The vacuum provided a suction pressure to keep the sediment sample in the tube. At this point the frit was unscrewed and removed; the tube was capped and sealed. A Dremel tool was employed to remove the top part of the tube from the top end of the sediment core, and the top end of the core was also capped and sealed.

All CT scanning of the sediment and cap was performed at the High-Resolution X-ray CT Facility at the University of Texas at Austin (UTCT). The CT equipment used was a custom-made CT unit manufactured by Bio-Imaging Research (BIR), Inc. (www.bio-imaging.com/). The X-ray source was a 200 kV FeinFocus model FXE 200.20, which is capable of a focal spot size less than 10 μm. The detector system was an image intensifier from which data were captured and digitized by a CCD 1024 × 1024 camera. All scans were done with X-ray peak energy at 150 kV and current between 0.21 and 0.25 mA. Each rotation consisted of 1000 angular positions (i.e., views), with an acquisition time of 0.133 sec per view. Data for multiple slices were acquired during a single specimen rotation by utilizing data off the true horizontal plane used for standard tomography. A slice-based reconstruction algorithm was used to produce one 16-bit TIFF image for each slice. Each slice had an interpixel spacing of 0.03271 mm and the interslice spacing was 0.03675 mm.

The 16-bit TIFF images were loaded into BLOB3D, an instrument detection limit-based program (Research Systems Inc., Boulder, CO) that was designed for processing three-dimensional CT datasets and extracting information concerning features or objects within the data volume. It was designed for efficient and rigorous definition, separation, and measurement of hundreds to tens of thousands of distinct and irregular objects from a data volume comprising tens to hundreds of megabytes. In this work, BLOB3D was used to uniquely separate, identify, and characterize each individual "macrovoid" within the sediment or cap. Note that the resolution of the CT system is insufficient to uniquely identify the individual grains and void spaces. Here we are using the word "void" to identify a subregion within the system that has a significantly different density than the surrounding material. Output from BLOB3D included the size and surface area of each individual void within the imaged subsection of the core. To make comparisons, a control sample was prepared. Twenty centimeters of sediment were placed into a glass cylinder and kept still for several weeks without methane injection. The sediment was cored using the same transparent plastic tube and scanned with CT equipment.

After removal of a core for CT scanning, a second sediment core was collected and sliced to determine the phenanthrene concentration profiles. Sections were obtained by placing the core on a post. The plastic tube was scaled and lowered 2 mm each section. A section was cut from the top of the extruded core with a knife and spatula.[29] Each section was split into two samples, one for moisture measurement and the other for contaminant analysis.

RESULTS AND DISCUSSION

Initial efforts were focused on high flow rates, typically much higher than might be expected with natural gas generation and release rates. This can provide an indication of mechanism of release but may overestimate quantitatively or qualitatively the effects of gas release.

Effects of Methane Flux on TSS or Sediment Flux

A movie recording bubble movement through the sediment-water interface was taken with a digital camera (Photron Motion Tools). The movie showed that the bubbles brought sediment particles into the water column upon leaving the sediment. The larger, heavier particles fell back to the sediment bed, whereas the smaller, lighter particles remained suspended in the water column. The experimental results show that TSS in the water column increased with time until it reached a constant value. Figure 2a shows the sediment fluxes with time at two different methane gas fluxes derived from TSS data. It is clear that the sediment flux to the water column increased with time in the beginning, reached a maximum value, and then gradually decreased to zero or a constant suspension-deposition equilibrium. The larger the methane flux, the higher the TSS or the sediment flux maximum value. This is understandable because the larger methane flux produces stronger forces on the particles resulting in larger final TSS.

Effects of Methane Flux and TSS or Sediment Flux on Contaminant Release

The experiments show that the phenanthrene concentration in the aqueous phase increased with time, reached a maximum value, and then decreased. This reflects the dynamics of the mass transfer processes occurring in the water column. Methane gas bubbles not only take up the contaminant from the pore water in the contaminated sediment but also suspend fine particulates in the water column. Both contaminated sediment particulates and methane gas bubbles release phenanthrene into the water. The driving force for mass transfer and phenanthrene desorption from gas bubbles and sediment particles is large in the beginning because phenanthrene concentration in the water is very small or near zero. This results in an increase in phenanthrene concentration in the water during the initial stages of the experiment. With time, the driving force decreases because of increasing aqueous phase concentration. As the methane gas bubbles transit the aqueous column they carry with them a certain fraction of phenanthrene to the overlying hexane layer.

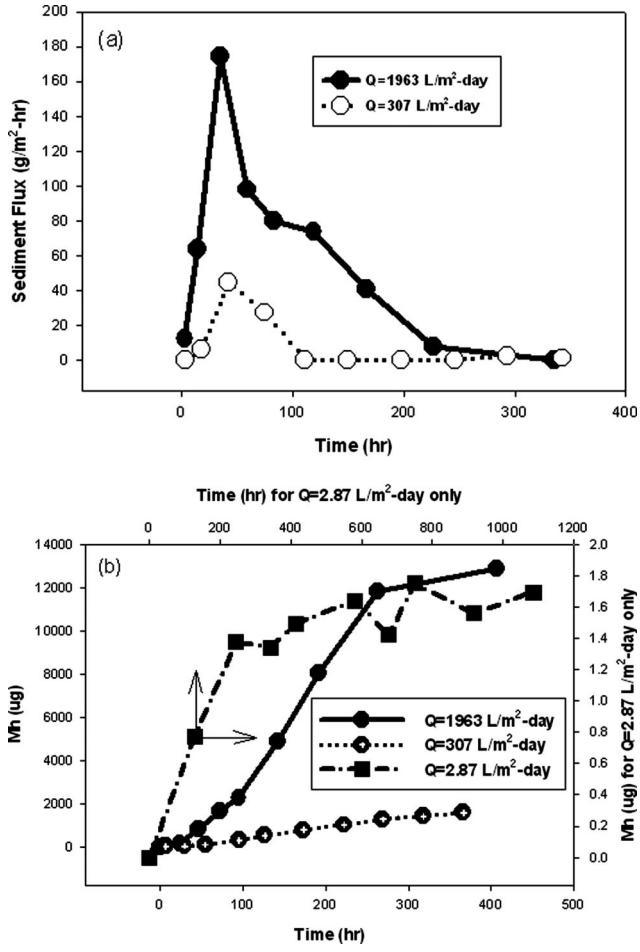

Figure 2. Sediment flux and phenanthrene mass in hexane (Mh) with time. (a) Sediment fluxes at two different methane fluxes; (b) Mh at three different methane fluxes.

When phenanthrene mass gain by desorption from sediment particles to water and the loss by gas bubble transport are equal, the peak value of the phenanthrene concentration is reached in the water. Eventually the phenanthrene concentration in the aqueous phase will decrease with time because the rate of mass gain by desorption from sediment particles becomes smaller than the rate of mass lost by bubble transport. The mass increase in the hexane layer with time shows a characteristic S-shape (Figure 2b). Phenanthrene mass in the hexane layer is mainly by methane bubble transport. In the beginning, the bubbles redistribute phenanthrene from pore water and release some into the water column. During this period, the phenanthrene mass increases slowly in the hexane layer. When the phenanthrene concentration in aqueous phase is high, the bubbles will transport phenanthrene from both the sediment pore water and the aqueous phase; that increases the mass increase in the hexane layer. Once the peak value of phenanthrene concentration in the aqueous phase is reached, bubbles will transport less mass as the concentration in the aqueous phase decreases with time. Thus the rate of mass increase in the hexane layer slows.

Methane flux influences the mass distribution of phenanthrene. A higher methane flux causes more sediment to be suspended in the water column and the peak

Table 1. Contaminant fluxes and effective MTCs at different methane fluxes.

Methane Flux mL/min (L/m^2·day)	Phenanthrene flux (N_A)[a] (μg/m^2·hr)	Effective MTC[b] (cm/yr)
6.85 (1963)	7069	80.11
1.07 (307)	877	9.94
0.01 (2.87)	0.42	0.0047
0.0035 (1)	0.15[c]	0.0017

Notes: [a]N_A is estimated by the slope of linear regression of the phenanthrene mass in hexane layer with time (Figure 2b) divided by the column cross section area. [b]Effective MTC = $N_A/(\rho_b W_s)$, where ρ_b is the sediment bulk density (kg/m^3) and W_s is the sediment loading (mg/kg). [c]This value is estimated at expected rates of gas release under field conditions (~1 l/m^2·day)[18] assuming that contaminant flux is a linear function of gas flow at low gas release rates.

value of phenanthrene concentration is reached earlier. It is obvious that the higher the flux of gas passing through the column, the more phenanthrene mass carried into the hexane. In fact, the total phenanthrene mass collected in the hexane layer is proportional to the methane gas flux.

One experiment with low methane flux (0.01 mL/min or 2.87 L/m^2·day) was conducted to simulate near field-flux conditions. The phenanthrene concentration in the water column was very small and undetectable, but the dissolved organic carbon (DOC) increased from 1.7 to 3.5 mg/L. The increase of phenanthrene mass in the hexane layer with time was extremely slow (Figure 2b). Phenanthrene fluxes and effective mass transfer coefficients (MTC) at various methane fluxes were estimated (Table 1). The effective MTC based on a solid phase sediment concentration of 0.0017 cm/yr at the lowest gas release rate can be compared with a typical bioturbation sediment reworking coefficient of the order of 0.1–10 cm/yr or higher.[30,31] Thus contaminant release due to gas ebullition is not expected to be significant relative to contaminant release from bioturbation in exposed contaminated sediments unless gas migration occurs at much higher rates than that associated with the natural evolution of gas as a byproduct of anaerobic degradation of organic matter. However, as indicated previously, the presence of contaminants in a liquid phase, either as a NAPL or soluble contaminants, could increase the proportion moved by gas release. The movement of contaminants by gas may also become the controlling release rate in capped systems, in which bioturbation is displaced to the surface of a cap rather than within the contaminated sediments.

Effect of Consolidation on Contaminant Release

For this experiment, the sediment was consolidated for 15 days before the methane gas was introduced into the column. Note that the methane flux was slightly lower in the experiment with sediment consolidation. Figure 3a shows that the time needed for the sediment flux to reach zero (i.e., TSS to reach a constant value) was around 95 hr for the unconsolidated sediment system, but increased to 343 hr for the consolidated sediment. The sediment consolidation can make the sediment more compact and harder to suspend. Because sediment suspension is a major phenanthrene release mechanism into the aqueous

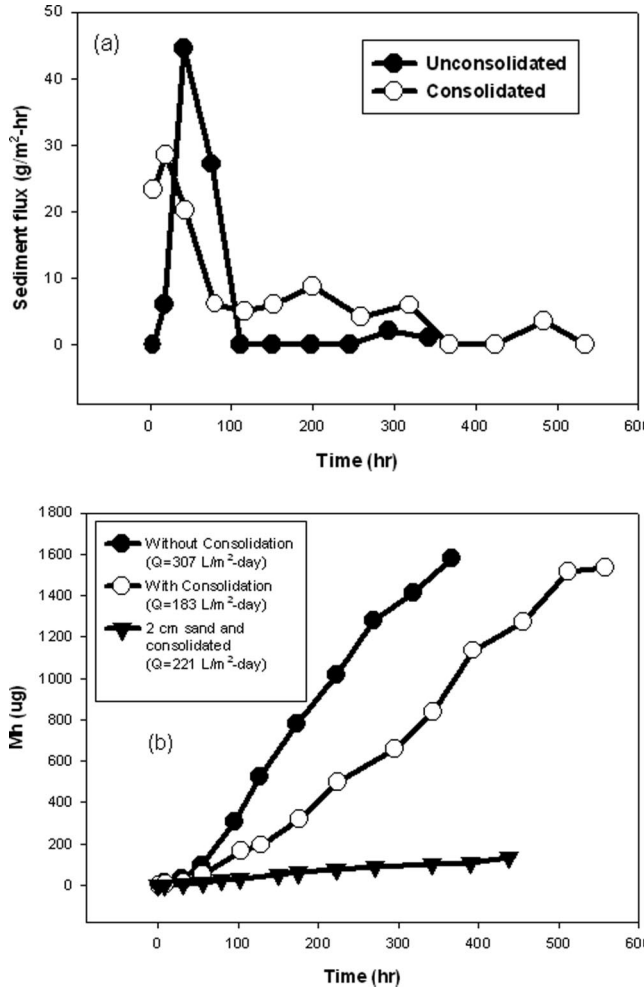

Figure 3. Sediment flux and phenanthrene mass in hexane (Mh) with time. (a) Sediment fluxes with and without consolidation; (b) Mh with and without cap.

phase and transport into the hexane layer, the delay in the TSS reaching a maximum for consolidated sediment system leads to the delay in the peak aqueous concentration and less phenanthrene mass in the hexane layer (Figure 3b).

Effect of Cap on Contaminant Release

A 2-cm sand cap was used to cap the contaminated, consolidated sediment. The stable phenanthrene concentration in the aqueous phase is approximately 5 ppb, around 5 times less than those for uncapped systems. The mass in the hexane layer for the capped sediment is also much smaller than those for the uncapped systems (Figure 3b). The reason is that the sand cap layer functions as a filter that effectively prevents sediment suspension. Although the water column became slightly turbid and the DOC in the aqueous phase increased from 1.3 to 5.7 mg/L, the TSS was too small to be measured using the filtration method. As stated earlier, the phenanthrene transport from the contaminated sediment to the water column and hexane layer was facilitated by bubbles in the uncapped case. For the capped system, although bubbles transported some phenanthrene, there was much less sediment suspended

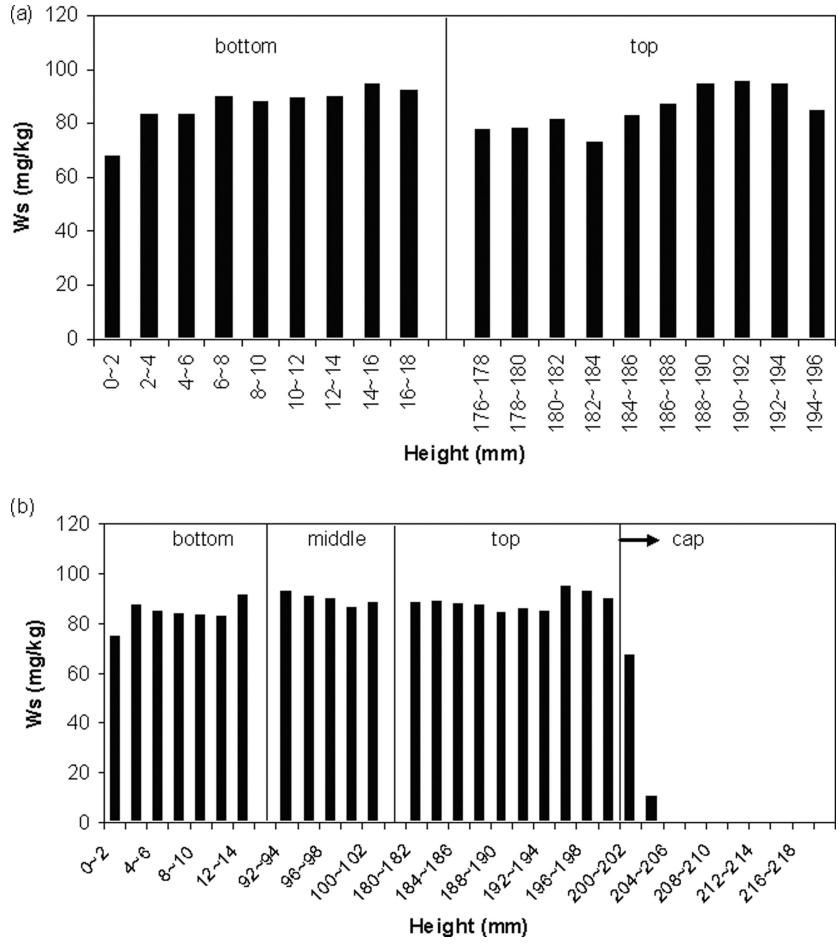

Figure 4. Phenanthrene concentration profile. (a) in sediment core (Q = 1.07 mL/min, 307 L/m^2·day); (b) in sediment and sand core (Q = 0.77 mL/min, 221 L/m^2·day).

in the water column. Hence, the water concentration of phenanthrene was very small.

Contaminant Concentration Profiles in Sediment Cores

The phenanthrene concentration profiles in all the sediment cores were measured. Figure 4a and b, shows two examples for capped and uncapped cores. The profiles demonstrate that there is a concentration decrease at the end of the sediment cores. At the top of the core, water, slurry, and sediment mixing tend to cause the concentration decrease. At the bottom of the core, phenanthrene transport from pore water into methane gas may be the reason for the concentration decrease. The concentration gradient between the pore water and the gas bubble should be larger at the column base because of the injection of clean methane. This can make phenanthrene concentration in the sediment decrease faster. No obvious concentration difference was observed in the middle of the sediment core. This may mean that bubbles circulated the pore water in the sediment. Pore water circulation in the sediment would make a uniform sediment loading possible. To confirm this hypothesis, further experiments should be done using CT to quantify the void distributions during methane injection. For capped cores, sediment and sand mixing at the sediment-sand interface was observed, which can be caused by the gas bubble movement and the density difference between sand and sediment.

Mass Balance

Total phenanthrene mass added with the sediment can be calculated by sediment loading and weight and water content that were measured when sediments were added to the column. During each experimental run, phenanthrene mass would redistribute in the sediment, slurry, and hexane layer. Phenanthrene mass in the hexane layer and in the aqueous phase are easily calculated using measured concentrations and volume. To estimate the phenanthrene mass on the soil particles in the slurry, an equilibrium partition coefficient, K_d, was used to calculate the phenanthrene concentration on the soil particles. This should not result in a large difference even if they are not at equilibrium because the phenanthrene mass in the slurry is only a very small part of the total phenanthrene mass. However, this practice can underestimate the phenanthrene mass on the sediment particles if there is no equilibrium between the aqueous phase and sediment. The particle weight can be estimated by TSS and slurry volume. The procedure to calculate the phenanthrene mass remained in the sediment is as follows.

The total phenanthrene remaining in the sediment can be calculated by

Table 2. Phenanthrene mass distribution in different phases and mass balance.

Cases	Total Mass Added with Sediment (mg)	Mass Distribution in Different Phases after the Experimental Run					
		Sediment (mg)	Slurry		Hexane Layer (mg)	Total Mass (mg)	Relative Error (%)
			Suspended Particles (mg)	Aqueous Phase (mg)			
Q = 6.85 mL/min (1963 L/m^2·day), t = 406.9 hr	56.6	39.8 (72.8%)	2.0 (3.6%)	0.07 (0.1%)	12.9 (23.5%)	54.7	3.6
Q = 1.07 mL/min (307 L/m^2·day), t = 366.5 hr	57.5	52.6 (96.4%)	0.3 (0.6%)	0.07 (0.1%)	1.6 (2.9%)	54.6	5.0
2 cm sand cap, Q = 0.77 mL/min (221 L/m^2·day), t = 473.5 hr	56.5	52.9 (98.5%)	0.6 (1.2%) (in sand)	0.02 (0.03%)	0.1 (0.3%)	53.7	4.9
Q = 0.64 mL/min (183 L/m^2·day), 15 days' sediment consolidation, t = 557.5 hr	56.0	49.5 (96%)	0.454 (0.9%)	0.07 (0.1%)	1.5 (3.0%)	51.5	8.0

$$m_s = \sum_{i=1}^{n} W_{si} V_{si} \rho_{bi} \quad (1)$$

where m_s is the phenathrene mass (mg) in the sediment, W_{si} is the sediment loading in the ith section (mg/kg), V_{si} is the volume of the ith section, ρ_{bi} is the sediment bulk density (kg/m^3), and n is the number of total sections, being equal to the total height of the sediment divided by the height of each section.

Usually sediment was sliced into several samples (2 mm each) from the top, middle, and bottom of the sediment core. As mentioned before, both sediment loading and moisture were measured. Sediment moisture can be used to estimate the sediment bulk density because the volume of each section is known. The sediment loading can be directly used in the above equation. For the other part of the middle area where there are no experimental data, the average of the loading from the middle (or several inside data from both top and bottom) was used. Because each sediment section is a conical frustum (on the bottom side) or a cylinder (on the top side), the sediment volume each section can be estimated by

$$V_{si} = \frac{\pi \cdot h_i}{12} (Dh_{i1}^2 + Dh_{i1} \cdot Dh_{i2} + Dh_{i2}^2) \quad (2)$$

where V_{si} is the volume of the section (m^3,) h_i is the height of the section (m), Dh_{i1} is the top diameter (m), and Dh_{i2} is the bottom diameter (m), which can be calculated by Dh = 5h/11 + 0.03 (m) for this specific column.

Table 2 lists the phenanthrene mass distributions for different cases. Each case gives a reasonably good mass balance. The data also indicate that methane flux is one major factor for phenanthrene mass distribution. Higher methane fluxes lead to more contaminant mass release from the sediment. The sand cap can be another major factor for phenanthrene mass distribution if the cap maintains its integrity.

Void Size Distribution in Sand and Sediment

Four separate sediment cores were imaged using CT. The first core was from the experiment at the high gas flow rate (Q = 6.85 mL/min, 1963 L/m^2·day), and the second one from the experiment with a lower gas flow rate (Q = 1.07 mL/min, 307 L/m^2·day). These two sediment cores were scanned in three regions each 3 mm thick. The top region begins 5 mm below the top, middle starts from the center of the sediment, and bottom starts 8 mm above the bottom. For the capped sediment core, four regions (6 mm each) were scanned, located at the middle of the sand layer and the top, the middle, and the bottom of the sediment. Only the middle part (6 mm) of the control sediment core was scanned. Qualitatively (see Figure 5, a, c, and d), it appears that there are a large number and better spatial distribution of void spaces in the experiments with methane injection compared with the control column. Quantitative analysis shows that the number of

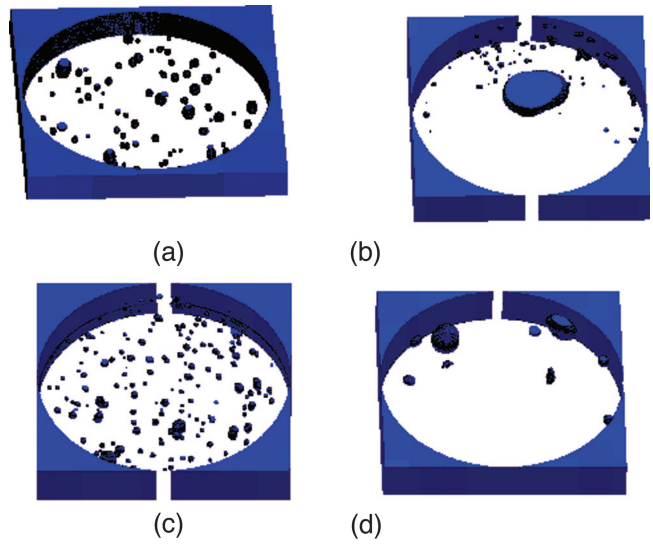

Figure 5. Images of void distributions. (a) in the middle of sediment core without cap (Q = 1.07 mL/min, 307 L/m^2·day); (b) in the middle of sand cap (Q = 0.77 mL/min, 221 L/m^2·day); (c) in the middle of sediment core with cap (Q = 0.77 mL/min, 221 L/m^2·day); (d) in the middle of the control sediment core (without methane gas flow).

Table 3. Void count and total volume for the different experimental conditions.

Sediment Specimens	Scanning Parts	Scanning Thickness (mm)	Number of Voids	Total Void Volume (mm^3)
The first core Q = 6.85 mL/min (1963 L/m^2·day)	Middle	3	94	59.0
	Bottom	3	61	35.2
The second core Q = 1.07 mL/min (307 L/m^2·day)	Middle	3	89	25.3
	Bottom	3	204	54.8
Capping sediment Q = 0.77 mL/min (221 L/m^2·day)	Sand layer	6	50	123.9
	Top	6	114	44.6
	Middle	6	160	28.5
	Bottom	6	35	20.5
Control sediment	Middle	6	7	54.6

voids in the column sediments is larger than in the control sediment (Table 3). This helps support our hypothesis that bubble migration enhances the pore water circulation within the sediment column and may help redistribute the void spaces. Analyses of the size distributions indicate that void spaces are smaller and more uniform at lower flow rates (Figure 5 and Table 3). Finally, a large 'bubble' or void space in the sand layer was observed (Figures 5b and 6b), suggesting the coalescence of the methane bubbles in the sand layer.

Contaminant Transport Pathway

Based on the above experimental observations, we postulate a pathway of gas bubble facilitated sediment and contaminant transport through sediment systems. For an uncapped system, organics in the contaminated sediment

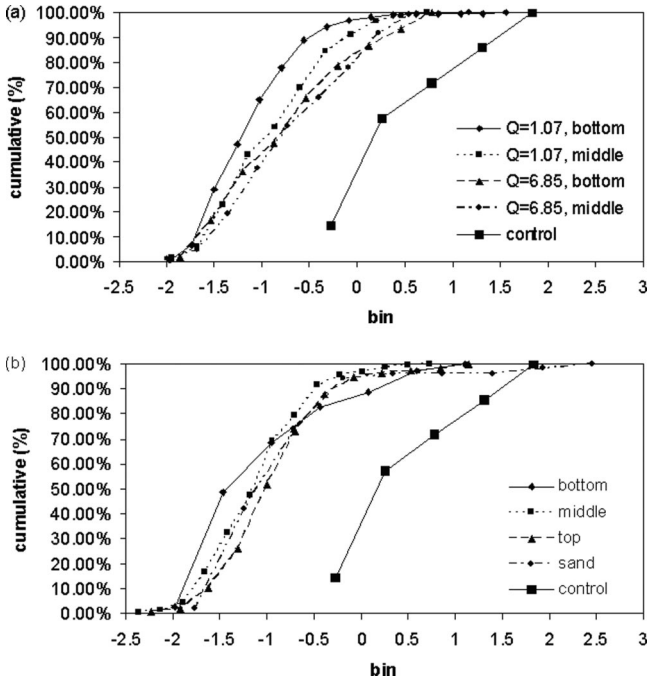

Figure 6. Void volume distributions (on a log scale): (a) in uncapped sediment and (b) in capped sediment/sand core.

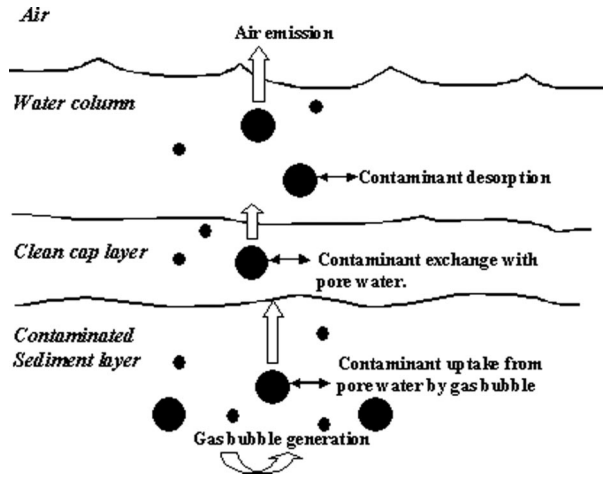

Figure 7. Depictions of gas bubble generation and migration through a cap.

can be converted into methane, carbon dioxide, and nitrogen gas by biological and microbial activities under anaerobic condition. Bubbles form with increasing gas vapor pressure. The bubbles take up contaminants from pore water in the contaminated sediment via gas/water partitioning and would move up into the water column when the pressure inside is larger than atmospheric plus hydrostatic pressure. We visually observed that the oblate bubbles (or ellipsoid) with their major (long) axis in the horizontal direction bring soil particles in their wake as they move through the sediment-water interface. The large/heavy particles would sink to the sediment and the small/light ones remain in the water column and form a slurry. The contaminated particles in the slurry will desorb contaminants into the aqueous phase and initially so will the bubbles. This increases the contaminant concentration in the aqueous phase. As the bubbles traverse the aqueous phase and break the surface, contaminants are released into the air. The experimental results clearly show that the sediment suspension is the major contaminant transport mechanism.

In the capped system (Figure 7), the bubbles generated in the contaminated sediment will move through the clean cap material. The gas bubbles release the contaminants into the pore water in the sand cap and water column. Although gas bubble movement may lead to some mixing of the sediment and sand at the sediment-sand interface, no significant sediment suspension is observed if the sand cap is not breached by the gas bubbles. In fact, the cap functions as a filter inhibiting sediment suspension, which eliminates or reduces the source of contaminant into the water column.

CONCLUSIONS

Partitioning and sediment suspension are two factors for contaminant transport associated with bubble ebullition in contaminated sediment. Experimental results show that sediment suspension is an important factor as a contaminant release mechanism. A sand cap can prevent or at least decrease the sediment suspension, making it a good barrier to bubble-facilitated contaminant release from contaminated sediments. At natural rates of gas generation and evolution in sediments (≤1 L/m^2·day), particle

resuspension rates and facilitated release rates of solid associated contaminants are relatively small. For example, bioturbation would be expected to give rise to far more rapid contaminant transport in stable uncapped sediments. CT images show that the bubble movement can redistribute the void spaces in the sediment and increase pore water circulation in the sediment, thus changing the sediment structure and integrity. Bubbles can also coalesce in the sand layer and large bubbles are more likely to break the sand cap. These factors should be considered in the design of caps over contaminated sediments in the field.

ACKNOWLEDGMENTS

This research was supported by a grant from EPA through the Hazardous Substances Research Center (South and Southeast) situated at LSU.

REFERENCES

1. Reible, D.D.; Constant, W.D.; Zhu Y. The Active Capping Demonstration Project in the Anacostia River, DC. Presented at the Third International Conference on Remediation of Contaminated Sediments. New Orleans, LA, January 24–27, 2005.
2. Huls, H.H.; Costello, M. Designing Assessments for Decision Making for Remediation of Contaminated Sediments. Presented at the Third International Conference on Remediation of Contaminated Sediments, New Orleans, LA, January 24–27, 2005.
3. Maynard, D.; Behrsing, J.; Crandell, C.; Kirkpatrick, G.; Vosburgh, J. Theory and Observations of DNAPL Migration in a Subaqueous Cap. Presented at the Third International Conference on Remediation of Contaminated Sediments. New Orleans, LA, January 24–27, 2005.
4. Valsaraj, K.T.; Yuan, Q.Z. Transport and Fate of Hazardous Substances in Capped Contaminated Sediment System. In *Abstract Book, Fourth SETAC World Congress and 25th Annual Meeting in North America, Portland, OR, USA, November 14–18 2004*, p 147.
5. Di Toro, D.M. *Sediment Flux Modeling*. Wiley-Interscience: New York, 2001.
6. Klaucke, I.; Sahling, H.; Bürk, D.; Weinrebe, W.; Bohrmann, G. Mapping Deep-Water Gas Emissions with Sidescan Sonar; *EOS Trans. Am. Geophys. Union* **2005**, *86,* 341-346.
7. Martens, C.S.; Klump, J.V. Biogeochemical Cycling in an Organic Rich Coastal Marine Basin-I. Methane Sediment-Water Exchange Processes; *Geochim. Cosmochim. Acta* **1980**, *44,* 471-490.
8. Hovland, M.; Judd, A.G. The Global Production of Methane From Shallow Submarine Sources; *Cont. Shelf Res.* **1992**, *12,* 1231-1238.
9. Johnson, B.D.; Boudreau, B.P.; Gardiner, B.S.; Maass, R. Mechanical Response of Sediments to Bubble Growth; *Marine Geol.* **2002**, *187,* 347-363.
10. Boudreau, B.P.; Gardiner, B.S.; Johnson, B.D. Rate of Growth of Isolated Bubbles in Sediments with a Diagenetic Source of Methane; *Limnol. Oceanog.* **2001**, *46,* 616-622.
11. Boudreau, B.P.; Gardiner, B.S.; Johnson, B.D. Rate of Growth of Isolated Bubbles in Sediments with a Diagenetic Source of Methane [Erratum to Document Cited in CA135:81463]; *Limnol. Oceanog.* **2001**, *46,* 1578.
12. Gardiner, B.S.; Boudreau, B.P.; Johnson, B.D. Growth of Disk-Shaped Bubbles in Sediments; *Geochim. Cosmochim. Acta* **2003**, *67,* 1485-14494.
13. Boudreau, P.B.; Algar, C.; Johnson, B.D.; Croudace, I.; Reed, A.; Furukawa, Y.; Dorgan, K.M.; Jumars, P.A.; Grader, A.S.; Gardiner, B.S. Bubble Growth and Rise in Soft Sediments; *Geology* **2005**, *33,* 517-520.
14. Tanner, C.C.; Adams, D.D.; Downes, M.T. Methane Emissions from Constructed Wetlands Treating Agricultural Wastewaters; *J. Environ. Qual.* **1997**, *26,* 1056-1062.
15. Rothfuss, F.; Conrad, R. Effect of Gas Bubbles on the Diffusive Flux of Methane in Anoxic Paddy Soil; *Limnol. Oceanog.* **1998**, *43,* 1511-1518.
16. Henry, P.; Thomas, M.; Clennell, M.B. Formation of Natural Gas Hydrates in Marine Sediments 2. Thermodynamic Calculations of Stability Conditions in Porous Sediments. *J. Geophys. Res. Atmos.* **1999**, *104,* 23005-230022.
17. Adams, D.D.; Naguib, M.; Brown, D.H. Cycling of Methane in Acidified Freshwater Environments; *Acid Rain* **1987**, *45,* 1-6.
18. Himmelheber, D.; Hughes, J. Complete Tetrachloroethene Dechlorination in Anacostia River Sediment. Presented at SETAC 26th Annual Meeting in North America, Baltimore, MD, November 13–17, 2005.
19. Fendinger, N.J.; Adams, D.D.; Glotfelty, D.E. the Role of Gas Ebullition in the Transport of Organic Contaminants from Sediments; *Sci. Total Environ.* **1992**, *112,* 189-201.
20. Van Kessel, T.; van Kesteren, W.G.M. Gas Production and Transport in Artificial Sludge Depots; *Waste Manage.* **2002**, *22,* 19-28.
21. Ketcham, R.A.; Carlson, W.D. Acquisition, Optimization and Interpretation of X-ray Computed Tomographic Imagery: Applications to the Geosciences; *Comput. Geosci.* **2001**, *27,* 381-400.
22. Jepsen, R.; McNeil, J.; Lick, W. Effects of Gas Generation on the Density and Erosion of Sediments from the Grand River; *J. Great Lakes Res.* **2000**, *26,* 209-219.
23. Selomulya, C.; Jia, X.; Williams, R.A. Direct Prediction of Structure and Permeability of Flocculated Structures and Sediments using 3D Tomographic Imaging. *Chem. Eng. Res. Des.* **2005**, *83,* 844-852.
24. Anderson, S.H.; Gantzer, C.J.; Boone, J.M.; Tully, R.J. Rapid Nondestructive Bulk Density and Soil-Water Content Determination by Computed Tomography; *Soil Sci. Soc. Am. J.* **1988**, *52,* 35-40.
25. Smith, J.S.; Valsaraj, K.T.; Thibodeaux, L.J. Bubble Column Reactor for Wastewater Treatment. 1. Theory and Modeling of Continuous Countercurrent Solvent Sublation; *Ind. Eng. Chem. Res.* **1996**, *35,* 1688-1699.
26. Smith, J.S.; Valsaraj, K.T. Bubble Column Reactors for Wastewater Treatment. 3. Pilot-Scale Solvent Sublation of Pyrene and Pentachlorophenol from Simulated Wastewater; *Ind. Eng. Chem. Res.* **1997**, *36,* 903-914.
27. Thoma, G.J. Ph.D. Dissertation, Louisiana State University, 1994.
28. American Public Health Administration/American Water Works Association/Water Environment Federation. *Standard Methods for the Examination of Water and Wastewater*. 18th ed.; American Public Health Association: Washington, DC, 1991.
29. Thoma, G.J.; Reible, D.D.; Valsaraj, K.T.; Thibodeaux, L.J. Efficiency of Capping Contaminated Sediments in Situ. 2. Mathematics of Diffusion-Adsorption in the Capping Layer; *Environ. Sci. Technol.* **1993**, *27,* 2412-2419.
30. Thibodeaux, L.J. *Environmental Chemodynamics: Movement of Chemicals in Air, Water, and Soil*. J. Wiley & Sons: New York, 1996.
31. Choi, J.; Francois-Carcaillet, F.; Boudreau, B.P. Lattice-Automation Bioturbation Simulator (LABS), Implementation for Small Deposit Feeders; *Comp. Geosci.* **2002**, *28,* 213-222.

About the Authors

Qingzhong Yuan is a doctoral candidate and Kalliat T. Valsaraj is a professor in the Department of Chemical Engineering at Louisiana State University. Danny D. Reible is a professor in the Department of Civil and Environmental Engineering at University of Texas. Clinton S. Willson is an associate professor in the Department of Civil and Environmental Engineering at Louisiana State University. Please address correspondence to: Kalliat T. Valsaraj, Department of Chemical Engineering, Louisiana State University, Baton Rouge, LA 70803; phone: +1-225-587-6522; fax: +1-225-578-1476; e-mail: valsaraj@lsu.edu.